AMERICAN SOCIETY FOR MICROBIOLOGY | Applied and Environmental Microbiology®

ENZYMOLOGY AND PROTEIN ENGINEERING

An 1,4-α-Glucosyltransferase Defines a New Maltodextrin Catabolism Scheme in *Lactobacillus acidophilus*

Susan Andersen,[a] Marie S. Møller,[a] Jens-Christian N. Poulsen,[b] Michael J. Pichler,[a] Birte Svensson,[a] Leila Lo Leggio,[b] Yong Jun Goh,[c] Maher Abou Hachem[a]

[a]Department of Biotechnology and Biomedicine, Technical University of Denmark, Kongens Lyngby, Denmark

[b]Department of Chemistry, University of Copenhagen, Copenhagen, Denmark

[c]Department of Food, Bioprocessing and Nutrition Sciences, North Carolina State University, Raleigh, North Carolina, USA

Susan Andersen and Marie S. Møller have contributed equally to the work. Susan Andersen initiated the study, and Marie S. Møller performed the final comprehensive phylogenetic analysis to conclude the work.

ABSTRACT The maltooligosaccharide (MOS) utilization locus in *Lactobacillus acidophilus* NCFM, a model for human small-intestine lactobacilli, encodes three glycoside hydrolases (GHs): a putative maltogenic α-amylase of family 13, subfamily 20 (*La*GH13_20), a maltose phosphorylase of GH65 (*La*GH65), and a family 13, subfamily 31, member (*La*GH13_31B), annotated as a 1,6-α-glucosidase. Here, we reveal that *La*GH13_31B is a 1,4-α-glucosyltransferase that disproportionates MOS with a degree of polymerization of ≥2, with a preference for maltotriose. Kinetic analyses of the three GHs encoded by the MOS locus revealed that the substrate preference of *La*GH13_31B toward maltotriose complements the ~40-fold lower k_{cat} of *La*GH13_20 toward this substrate, thereby enhancing the conversion of odd-numbered MOS to maltose. The concerted action of *La*GH13_20 and *La*GH13_31B confers the efficient conversion of MOS to maltose that is phosphorolyzed by *La*GH65. Structural analyses revealed the presence of a flexible elongated loop that is unique for a previously unexplored clade of GH13_31, represented by *La*GH13_31B. The identified loop insertion harbors a conserved aromatic residue that modulates the activity and substrate affinity of the enzyme, thereby offering a functional signature of this clade, which segregates from 1,6-α-glucosidases and sucrose isomerases previously described within GH13_31. Genomic analyses revealed that the *La*GH13_31B gene is conserved in the MOS utilization loci of lactobacilli, including acidophilus cluster members that dominate the human small intestine.

IMPORTANCE The degradation of starch in the small intestine generates short linear and branched α-glucans. The latter are poorly digestible by humans, rendering them available to the gut microbiota, e.g., lactobacilli adapted to the small intestine and considered beneficial to health. This study unveils a previously unknown scheme of maltooligosaccharide (MOS) catabolism via the concerted activity of an 1,4-α-glucosyltransferase together with a classical hydrolase and a phosphorylase. The intriguing involvement of a glucosyltransferase likely allows the fine-tuning of the regulation of MOS catabolism for optimal harnessing of this key metabolic resource in the human small intestine. The study extends the suite of specificities that have been identified in GH13_31 and highlights amino acid signatures underpinning the evolution of 1,4-α-glucosyl transferases that have been recruited in the MOS catabolism pathway in lactobacilli.

KEYWORDS carbohydrate metabolism, *Lactobacillus*, disproportionating enzyme, gut microbiota, maltooligosaccharides, microbiota, oligosaccharide 1,4-α-glucanotransferase, prebiotic, probiotic, starch

Citation Andersen S, Møller MS, Poulsen J-CN, Pichler MJ, Svensson B, Lo Leggio L, Goh YJ, Abou Hachem M. 2020. An 1,4-α-glucosyltransferase defines a new maltodextrin catabolism scheme in *Lactobacillus acidophilus*. Appl Environ Microbiol 86:e00661-20. https://doi.org/10.1128/AEM.00661-20.

Editor Isaac Cann, University of Illinois at Urbana-Champaign

Address correspondence to Leila Lo Leggio, leila@chem.ku.dk, or Maher Abou Hachem, maha@bio.dtu.dk.

Received 17 March 2020
Accepted 12 May 2020
Accepted manuscript posted online 22 May 2020
Published 20 July 2020

Humans have coevolved with a diverse and vast bacterial community (1), termed the human gut microbiota (HGM), which exerts considerable effects on our health as well as metabolic and immune homeostasis (2). The gut microbiota confers metabolic activities that are not encoded by the human genome, e.g., the bioconversion of xenobiotics (3) and harvesting of energy from nondigestible glycans (4). The most prevalent and abundant gut bacterial phyla in healthy adults are *Firmicutes*, *Bacteroidetes*, and *Actinobacteria* (5, 6). Complex chemical and physical gradients provide diverse ecological and metabolic niches along the gastrointestinal tract, thereby defining a biogeography for different HGM taxa. Thus, the small intestine is enriched with bacteria from the Gram-positive *Firmicutes* phylum, *Lactobacillaceae* family (6), especially *Lactobacillus* spp., which are ascribed health-promoting properties (7, 8).

Lactobacillus acidophilus NCFM is one of the best-characterized models for acidophilus cluster human gut lactobacilli (7, 9). This strain has been used commercially as a probiotic and synbiotic, owing to its suggested potential in improving intestinal transit during constipation as well as mucosal functions in healthy elderly people (10, 11). The adaptation of *L. acidophilus* NCFM to the small intestine, which is rich in dietary carbohydrates, is highlighted by the numerous carbohydrate-specific transporters and intracellular carbohydrate active enzymes (CAZymes; http://www.cazy.org/ [12]) encoded by this bacterium. The genetic and molecular basis for the high saccharolytic capacity of *L. acidophilus* NCFM has been explored for a range of nondigestible di- and oligosaccharides (13, 14) as well as plant glycosides (15).

Starch from cereals, tubers, roots, and rhizomes dominates human caloric intake (16). Digestion of starch by human salivary and pancreatic α-amylases results in significant amounts of maltooligosaccharides (1,4-α-gluco-oligosaccharides; MOS) and 1,6-α-branched limit dextrins, the latter being recalcitrant to digestion by human digestive enzymes. Therefore, these oligosaccharides represent an abundant metabolic resource for bacteria that colonize the small intestine. Starch metabolism is relatively well-studied in colonic microbiota members of, e.g., *Bacteroides* and *Clostridia* (17, 18). In contrast, α-glucan metabolism by lactobacilli that dominate the small intestine has received less attention.

Recently, we have shown that the utilization of short, branched α-glucans from starch degradation by *L. acidophilus* NCFM is conferred by a cell-attached 1,6-α-debranching enzyme (*La*Pul13_14) (19). The MOS products from this enzyme or from human starch breakdown are likely internalized by an ATP-binding cassette transporter, which is conserved in MOS utilization gene clusters in lactobacilli together with amylolytic and catabolic enzymes (gene locus tags LBA1864 to LBA1874 in *L. acidophilus* NCFM) (Fig. 1), and the activity of a glycoside hydrolase family 65 maltose phosphorylase (*La*GH65, LBA1870; EC 2.4.1.8) has been demonstrated (20). Another conserved gene within this locus (LBA1872) (Fig. 1) is currently annotated as an oligo-1,6-α-glucosidase belonging to GH13 subfamily 31 (GH13_31). We have previously described another functional GH13_31 glucan-1,6-α-glucosidase from *L. acidophilus* (*La*GH13_31A) (21), which raised questions regarding the function and organization of the LBA1872 gene within the MOS utilization locus of *L. acidophilus*.

In this study, we demonstrate that LBA1872 from *L. acidophilus* NCFM encodes a MOS disproportionating enzyme (1,4-α-glucosyltransferase, here termed *La*GH13_31B) with a preference for maltotriose (M3). The reaction scheme of *La*GH13_31B uses an MOS with n glucosyl units both as a donor and an acceptor, yielding two products, one with an $n - 1$ unit and one with an $n + 1$ unit. Sequence and structural analyses have revealed a dynamic loop that modulates the activity and substrate affinity of the enzyme, thereby offering a functional signature of this specificity. We expressed and kinetically characterized the two remaining GHs in the MOS utilization locus (*La*GH65/LBA1870 and *La*GH13_20/LBA1871) in *L. acidophilus* NCFM and showed that *La*GH13_31B acts in concert with these enzymes to enable the efficient breakdown of MOS.

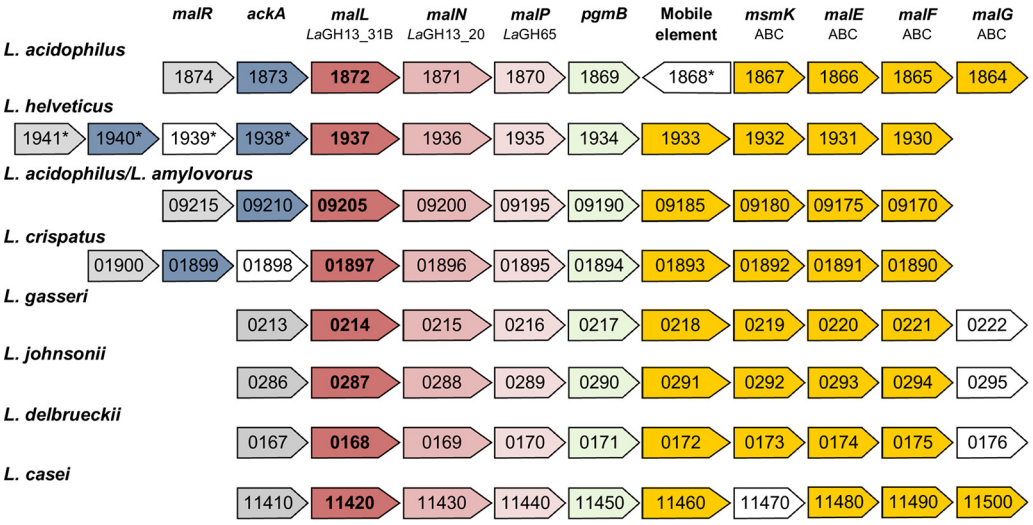

FIG 1 Organization of maltooligosaccharide utilization loci in gut *Lactobacillus* strains. The numbers indicate gene locus tags of the first strain mentioned in the following clusters: *L. acidophilus*, *L. acidophilus* NCFM and *L. acidophilus* La-14; *L. helveticus*, *L. helveticus* H10, *L. helveticus* CNRZ32, *L. helveticus* R0052, and *L. helveticus* DPC 4571; *L. amylovorus*/*L. acidophilus*, *L. acidophilus* 30SC, *L. amylovorus* GLR1118, and *L. amylovorus* GLR1112; *L. crispatus*, *L. crispatus* ST1; *L. gasseri*/*L. johnsonii*, *L. johnsonii* FI9785, *L. gasseri* ATCC 33323, *L. johnsonii* N6.2, *L. johnsonii* DPC6026, and *L. johnsonii* NCC533; *L. delbrueckii*, *L. delbrueckii* subsp. *bulgaricus* and *L. delbrueckii* subsp. *bulgaricus* ND02; *L. casei*, *L. casei* BL23, *L. casei* LOCK91, *L. casei* Zhang, *L. casei* BD-II, *L. casei* ATTCC 334, and *L. casei* LCZW. Colors indicate transcriptional regulators (light gray), acetate kinases (blue), *La*GH13_31B orthologues (boldface and red), *La*GH13_20 orthologues (pink), *La*GH65 orthologues (light pink), β-phosphoglucomutase (green), and components of an ATP-binding cassette transporter (orange). Genes with the following products are shown in white: transposase (1868 and 1939), hypothetical protein (01898), and α-1,6-glucosidase (11470, 0295, and 0176). Asterisks indicate elements not present in any of the published genomes.

RESULTS

The MOS utilization gene cluster in *L. acidophilus* NCFM encodes a disproportionating enzyme. *La*GH13_31B was not active toward panose and isomaltose, which are diagnostic of α-(1, 6)-glucosidase activity (see Fig. S1 in the supplemental material). In contrast, *La*GH13_31B disproportionated MOS with a degree of polymerization (DP) of 2 to 7 (M2 to M7) by one glucosyl moiety (Fig. S2A and B), and no hydrolysis products were observed. The enzyme had similar equilibrium activity profiles on M3 through M7, while M2 was a poor substrate (Fig. S2B). Moreover, the presence of amylose (DP17) or glycogen did not alter the activity profiles (Fig. S2C), establishing the specificity of *La*GH13_31B as an oligosaccharide-specific 1,4-α-glucosyltransferase. Coupled enzyme assays and high-pH anion-exchange chromatography with pulsed amperometric detection (HPAEC-PAD) were used to measure the apparent kinetic parameters of disproportionation by *La*GH13_31B, using M2 to M4 as substrates (Table 1 and Fig. S3). The best substrate (coupled enzymatic assay) was M3, owing to a higher k_{cat} than those for both M2 and M4. Similar K_m and catalytic efficiency (k_{cat}/K_m) values on M4 were found by the coupled enzymatic assay and HPAEC-PAD analysis (Table 1). A roughly 3-fold

TABLE 1 Kinetic parameters of enzymes in the maltodextrin utilization gene cluster in *L. acidophilus* NCFM[a]

	1,4-α-Glucosyltransferase (*La*GH13_31B)			Maltogenic α-amylase (*La*GH13_20)			Phosphorylase (*La*GH65)		
Substrate	K_m (mM)	k_{cat} (s^{-1})	k_{cat}/K_m (s^{-1} mM^{-1})	K_m (mM)	k_{cat} (s^{-1})	k_{cat}/K_m (s^{-1} mM^{-1})	K_m (mM)	k_{cat} (s^{-1})	k_{cat}/K_m (s^{-1} mM^{-1})
M2	79 ± 6	0.9 ± 0.0	0.01				3.0 ± 0.3	69 ± 3	23
M3	6.5 ± 1.4 4.8 ± 1.4[b]	424 ± 50 102 ± 18[b]	65 21[b] (0.16)[c]	2.9 ± 1.1	9.7 ± 0.7	3.3			
M4	8.1 ± 1.0[b]	325 ± 12[b]	40[b]	0.8 ± 0.1	117 ± 9	146			

[a]See Fig. S3 for Michaelis-Menten plots and Fig. 6 for the reactions catalyzed by these enzymes.
[b]Measured by HPAEC-PAD.
[c]Transferase kinetics of *La*GH13_31B Y295A on M3 obtained from single-time-point incubations (5 min) as presented in Fig. 5B.

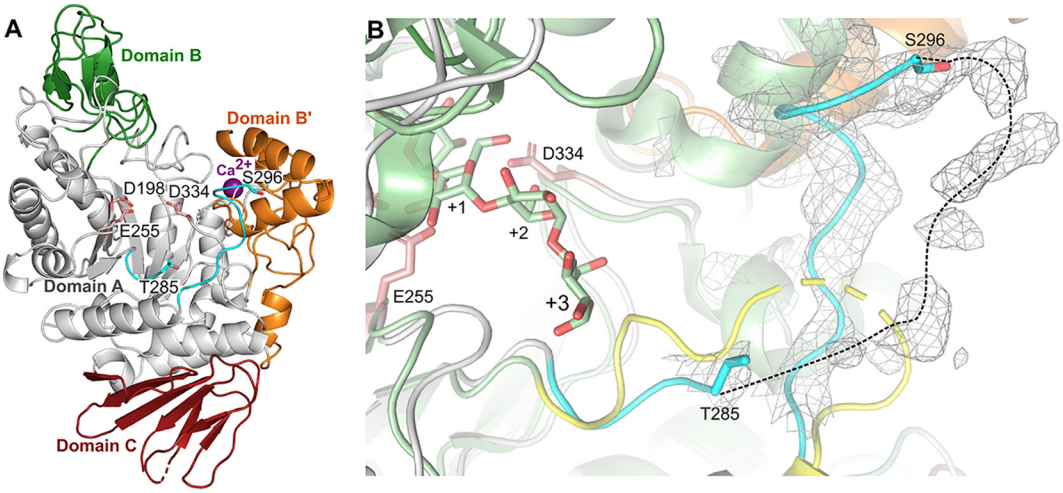

FIG 2 (A) Overall structure of *La*GH13_31B. Domain A (residues 3 to 100, 170 to 373, and 458 to 477, gray), domain B (residues 101 to 169, green), domain B′ (residues 373 to 457, orange), and domain C (residues 478 to 550, red) are shown. The catalytic residues (nucleophile, D198; general acid/base, E255; transition state stabilizer, D334) are in light red, and Ca^{2+} is a purple sphere. The long loop at the entrance to the active site having a disordered segment (residues 286 to 295) is in cyan, and residues before and after the unmodelled part are in cyan sticks. (B) Close-up view of the disordered loop region in panel A. *La*GH13_31B is in a similar orientation and color as those in panel A but slightly tilted to visualize the partial electron density trace. The closest structural homologue from *Bacillus*, *Bsp*AG13_31A (PDB entry 5ZCE; light green, with the loop corresponding to the disordered loop of *La*GH13_31B in yellow; maltotetraose is shown in light green sticks) is superimposed on *La*GH13_31B for comparison. The disordered loop is likely to be flexible, allowing substrate-induced closure and possibly aromatic stacking via a conserved Y/F that clamps the substrate similarly to other transferases of GH13 or GH77. Electron density at the +1.0 σ level is in gray mesh to highlight the disordered loop insertion in *La*GH13_31B. The plausible conformation of the disordered loop is shown as a dashed line.

higher k_{cat}/K_m was obtained on M3 as the substrate using the coupled enzyme assay than with the HPAEC assay (Table 1), suggesting that the production of M2 in the reaction affects the reaction kinetics. Notably, the catalytic efficiency (k_{cat}/K_m) on M2 was about 4,700-fold lower than that of M3, owing to a very high K_m for M2 (Table 1).

Enzymology of MOS degradation in *L. acidophilus* NCFM. To dissect the role of *La*GH13_31B in MOS metabolism, we carried out kinetic analyses on the maltose phosphorylase *La*GH65 and the maltogenic α-amylase *La*GH13_20, both encoded by the same MOS locus as *La*GH13_31B (Fig. 1). The efficiency of *La*GH65 on M2 was 1,500-fold higher than that of *La*GH13_31B (Table 1). Comparing the efficiency of *La*GH13_20 and *La*GH13_31B on M3 and M4 revealed that these enzymes had a reciprocal preference. While M3 was a fairly poor substrate for *La*GH13_20, owing to a low k_{cat}, the efficiency of *La*GH13_31B toward this substrate was 20-fold higher (coupled assay) due to a 44-fold higher k_{cat} (Table 1). Conversely, M4 was the preferred substrate for *La*GH13_20 compared to *La*GH13_31B, owing mainly to a 10-fold lower K_m. Finally, the action of *La*GH13_31B on MOS in the presence of both *La*GH65 and *La*GH13_20 was tested using HPAEC-PAD analysis (Fig. S4). The mixture resulted in efficient breakdown and the accumulation of maltose and some glucose, which was not observed for *La*GH13_31B alone.

***La*GH13_31B displays a more open active site with a potentially dynamic loop than GH13_31 hydrolases.** The structure of *La*GH13_31B is the first to represent the 1,4-α-glucosyltransferase activity within GH13_31. *La*GH13_31B shares the catalytic machinery and the overall domain structure of amylolytic GH13 enzymes, namely, a $(\beta/\alpha)_8$ catalytic domain A (residues 1 to 477; catalytic residues D198, E255, and D334), with two inserted domains (domain B, residues 100 to 169; domain B′, residues 373 to 457), and a domain C, composed primarily of β-sheets (478 to 550) (Fig. 2A). A Ca^{2+} binding site formed by side chains of D20, N22, D24, and D28 and main-chain carbonyls of I26 and H73 is identified in a location similar to that of counterparts present in some GH13_31 structures (22).

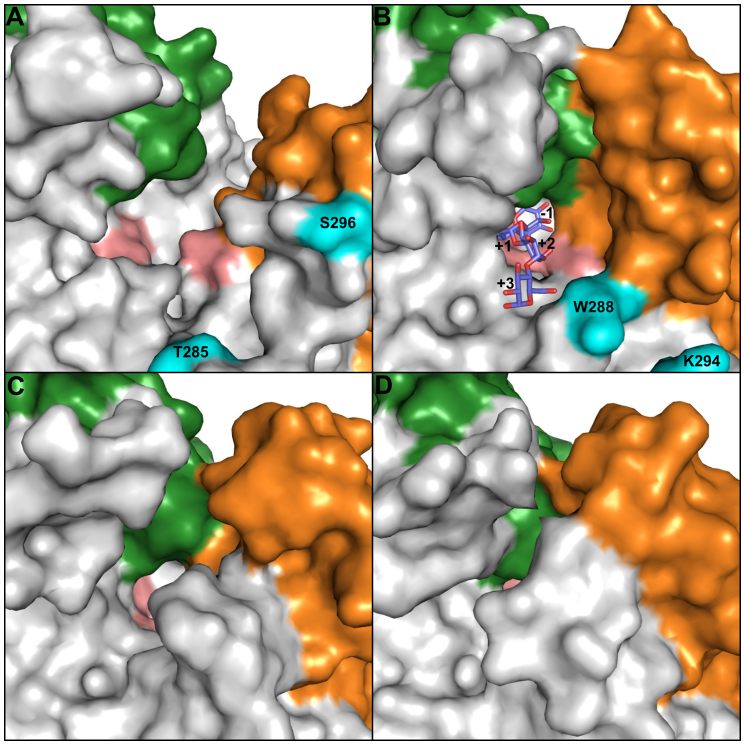

FIG 3 Comparison of the orientation of the B′ domain of selected GH13_31 structures. (A) *La*GH13_31B (PDB entry 6Y9T). (B) *Bsp*AG13_31A (PDB entry 5ZCE) with M4 as blue sticks and subsites labeled. (C) Oligo-1,6-α-glucosidase from *Bacillus cereus* (PDB entry 1UOK). (D) α-Glucosidase (sucrase-isomaltase-maltase) from *Bacillus subtilis* (PDB entry 4M56). The view is as described for Fig. 2A. Shown are domain A (gray), domain B (green), domain B′ (orange), domain C (red), and catalytic residues (light red). Residues at both sides of unsolved loop regions are in cyan.

A DALI search identified a GH13 subfamily 29 trehalose-6-phosphate hydrolase (PDB entry 5BRQ) as the closest structural homologue to *La*GH13_31B, closely followed by GH13_31 enzymes, all sharing 32 to 36% sequence identity (Table S1). Based on a phylogenetic analysis of GH13_31 sequences from lactobacilli and characterized GH13_31 members (see Fig. 4A), the recently characterized α-glucosidase from *Bacillus* species, *Bsp*AG13_31A (22), and a *Geobacillus* α-glucosidase (23) were the closest structurally characterized enzymes.

A clear difference from other GH13_31 structures is the positioning of domain B′, which is tilted away from the catalytic domain to create a more open cleft-like active site in *La*GH13_31B. In contrast, in the GH13_31 hydrolases, domain B′ packs closely onto the catalytic domain, resulting in a pocket-shaped active-site architecture (Fig. 3).

Electron density was lacking for a long loop at the entrance to the active site, hence, residues 286 to 295 are not modeled in the structure. Notably, the corresponding but shorter loop in *Bsp*AG13_31A (Fig. 2B) was suggested to be flexible based on the poor electron density and ligand binding-dependent conformational changes in this loop (22).

Sequence alignment and phylogenetic analysis. To map the taxonomic distribution of *La*GH13_31B-like sequences and to identify possible functional signatures of the transferase activity, we performed a sequence and phylogenetic analysis. *La*GH13_31B and close homologues segregate in a distinct clade populated by *Lactobacillus* sequences (Fig. 4A), and the genes encoding these sequences are exclusively organized as *La*GH13_31B in MOS utilization loci (Fig. 1). Sequences populating the *La*GH13_31B clade lack the signature of 1,6-α-glucosidases within region II of GH13 enzymes, i.e., a valine following the catalytic nucleophile, and they possess a region V motif resembling neopullulanase (α-1,4-hydrolase) instead of 1,6-α-glucosidase (24), consistent with the

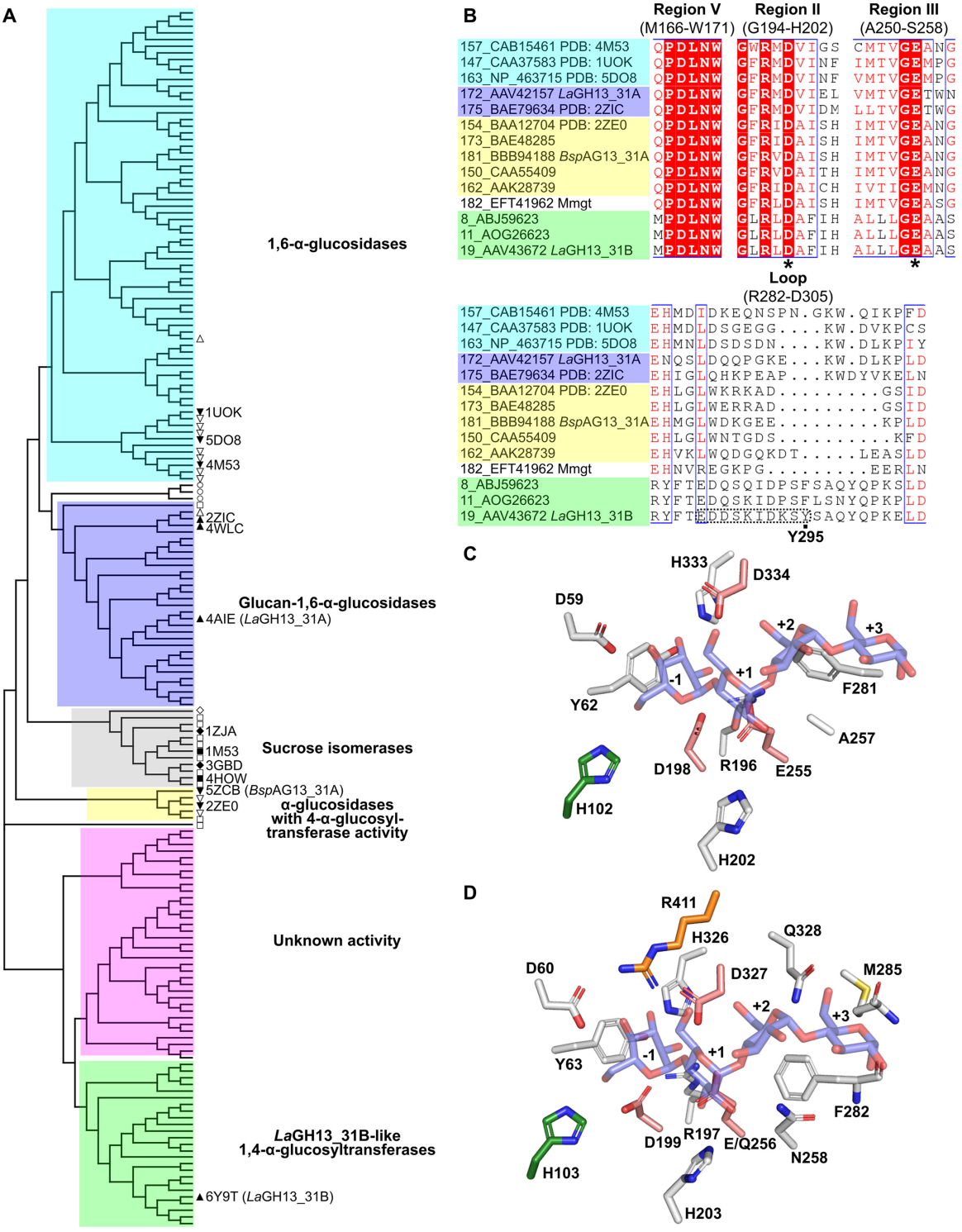

FIG 4 (A) Phylogenetic tree of GH13_31 based on a structure-based alignment of 183 sequences from lactobacilli and characterized GH13_31 enzymes from the CAZy database (accession numbers and taxonomic origins are in Table S2 and Fig. S5). Characterized GH13_31 sequences are labeled according to the taxonomic order of the source organism (△, *Lactobacillales*; ▽, *Bacillales*; ○, *Bifidobacteriales*; □, *Enterobacterales*; ◇, other *Gammaproteobacteria*). Solid labels and a PDB entry denote structurally characterized members. (B) Excerpts of conserved GH13 regions II, III (48), and V (24), including selected characterized sequences and two additional members of the *La*GH13_31B clade from *L. gasseri* and *L. johnsonii* (see Fig. S5 for full alignment). The catalytic nucleophile and the general acid/base are indicated by asterisks. An excerpt of the Y295A-harboring loop of *La*GH13_31B is shown. The disordered loop segment in *La*GH13_31B is indicated. (C and D) Comparison of *La*GH13_31B (C) and *Bsp*AG13_31A (D) (PDB entry 5ZCE) active-site residues. The coloring is as described for Fig. 2A, and M4 from *Bsp*AG13_31A (PDB entry 5ZCE) is in blue sticks.

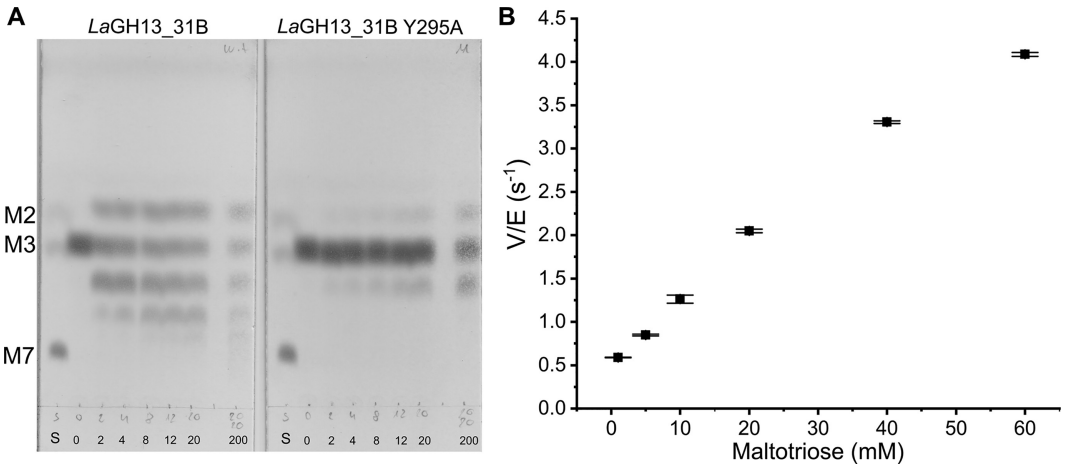

FIG 5 Comparison of activity of *La*GH13_31B and its Y295A mutant. (A) TLC of transferase activity of *La*GH13_31B and its Y295A mutant (both at 0.5 μM) on M3 (10 mM), showing reduced activity of the mutant compared to that of the wild type on M3 over time (0, 2, 4, 8, 12, 20, and 200 min; S, standard of M2, M3, and M7). (B) Transferase kinetics of *La*GH13_31B Y295A on M3 showing the means with standard deviations from triplicates.

α-1,4-linkage activity (Fig. 4B). Another distinguishing feature is the occurrence of small amino acid residues following the catalytic general acid/base in the conserved region III (Fig. 4B), which results in a more open entrance to the active site of *La*GH13_31B than that of 1,6-α-glucosidases. The region III substitutions translate into fewer potential substrate contacts at subsites +2 and +3 in *La*GH13_31B than in *Bsp*AG13_31A (PDB entry 5ZCE), e.g., N258 at subsite +2 of *Bsp*AG13_31A is replaced by A257 in *La*GH13_31B (Fig. 4C and D).

Another interesting feature of the *La*GH13_31B clade is an insertion in a loop region (R282-D305) that harbors a conserved aromatic residue (Y295, *La*GH13_31B numbering), which is absent from the sequences of enzymes of other specificities within GH13_31 (Fig. 4B and Fig. S5). Interestingly, this loop is in the same region and is disordered in the crystal structure of *La*GH13_31B described above (Fig. 2B), which may substitute for the paucity of substrate interactions at subsites +2 and +3 in *La*GH13_31B compared to that of *Bsp*AG13_31A (Fig. 4C and D).

The unique extended loop of *La*GH13_31B contributes to substrate binding affinity. To examine the functional role of the distinctive loop insertion and the conserved Y295 in *La*GH13_31B, we mutated this residue to alanine. The mutant had an unfolding profile similar to that of the wild-type enzyme, precluding a gross change in the overall folding and stability (Fig. S6). The activity on M3 was greatly reduced, and no disproportionation products larger than M4 were observed in the thin-layer chromatography (TLC) analysis (Fig. 5A). The loss of activity was confirmed by specific activity measurements and was more severe for larger substrates based on 40-fold and 140-fold loss of specific activity on M2 and M3, respectively, using the coupled assay. Moreover, the severely reduced k_{cat}/K_m on M3 (Table 1), along with the loss of curvature in the kinetic data, suggest a substantial loss in substrate affinity (Fig. 5B and Fig. S3). These data support an important role of the flexible loop and the conserved aromatic residue it harbors in substrate binding. This loop may provide favorable binding interactions to define a dominant +2 subsite that governs clamping the substrate at this site, which would favor unproductive binding of M2 at subsites +1 and +2. This is consistent with the high K_m on M2 and the excellent affinity to M3, as well as the larger reduction of activity toward M3 than M2 for the *La*GH13_31B Y295A mutant.

DISCUSSION

Lactobacilli are industrially important and diverse bacteria that colonize a multitude of ecological niches, including water, soil, fermented material (plant, meat, and dairy), and gastrointestinal tracts of humans and animals. *L. acidophilus* and closely related

species from the acidophilus group are adapted to the small intestine of humans, where α-glucans from starch breakdown are an abundant metabolic resource (6, 19).

Previously, the maltose phosphorylase *La*GH65, encoded by the MOS gene cluster in *L. acidophilus* NCFM, was characterized (20), in addition to a glucan-1,6-α-glucosidase (*La*GH13_31A) from the same strain (21). However, the role of LBA1872, residing in the MOS gene cluster (Fig. 1), remained unclear. The LBA1872 gene product shares amino acid sequence similarities to 1,6-α-glucosidases (37% identity to *La*GH13_31A) (21) and to a recently described disproportionating 1,4-α-glucosyltransferase from *Enterococcus faecalis* (MmgT; 35% identity) (25), which was only qualitatively described using thin-layer chromatography. The tentative functional assignment prompted us to express LBA1872 (*La*GH13_31B) as well as the two other 1,4-α-active enzymes from the MOS gene cluster from *L. acidophilus* NCFM to investigate the roles of these enzymes in MOS metabolism.

***La*GH13_31B populates a distinct clade in GH13_31, which is defined by a unique loop insertion harboring a conserved aromatic residue.** The valine residue following the catalytic nucleophile in the conserved region II in 1,6-α-glucosidases of GH13_31 (26) is replaced with alanine in *La*GH13_31B (Fig. 4B; see also Fig. S5 in the supplemental material) (21), consistent with the lack of activity of the latter enzyme toward 1,6-α-glucans. Our present phylogenetic tree showed that *La*GH13_31B defines a distinct clade that segregates from characterized GH13_31 members (Fig. 4A) and that is populated solely by sequences from lactobacilli. We identified a unique insertion in the loop region between R282 and D305 (*La*GH13_31B numbering) that is lacking in GH13_31 sequences from other clades (Fig. 4). This loop harbors a tyrosine (Y295) that is chemically conserved (Y or F) within the inspected homologues (Fig. 4B and Fig. S5). The mutational analysis showed that Y295 from this loop is important for activity and substrate affinity based on the loss of the curvature of transferase activity on the preferred substrate, M3 (Fig. 5B and Fig. S3). The poor or lacking electron density for parts of this loop in *La*GH13_31B are suggestive of its high flexibility. Flexible loops that present substrate-binding aromatic residues have been observed in other transferases, e.g., the GH13 4-α-glucanotransferase from *Thermotoga maritima*, which can convert starch, amylopectin, and amylose by transferring maltosyl and longer dextrinyl residues to MOS. This 4-α-glucanotransferase harbors an aromatic "clamp," which captures substrates at the +1 and +2 subsites (27). In addition, flexible loops that undergo considerable conformational changes during the catalytic cycle have also been identified in 4-α-glucanotransferases of GH77 from *Thermus brockianus* (28), *Escherichia coli* (29), and *Arabidopsis thaliana* (30). In particular, the 4-α-glucanotransferase from *T. brockianus* was shown to possess an aromatic residue (F251) located on the flexible loop that binds substrates at subsites +1 and +2 (28). The observed functional role of the flexible loop in *La*GH13_31B assigns it as a unique descriptor of the *La*GH13_31B clade that is conserved within the MOS utilization loci in *Lactobacillus*.

***La*GH13_31B acts as an enzymatic pivot in the metabolism of maltodextrins in *L. acidophilus* NCFM.** The characterization of *La*GH13_31B provides compelling evidence on the 1,4-α-glucosyltransferase activity of the enzyme. The kinetics of disproportionation revealed an exceptionally low activity on M2 and an increase in k_{cat}/K_m on M3 of at least 3 orders of magnitude (Table 1). This difference suggests that the binding of M2 at subsites −1 and +1 is not favorable. In contrast, the roughly 6- to 9-fold decrease in K_m when M3 is used as an acceptor is consistent with a key role of subsite +2 and the preferred binding mode between subsites −1 through +2, likely promoted by the additional interactions with the flexible loop discussed above. The preference for M3 is complementary to that of *La*GH13_20, which displays about a 40-fold preference for M4 compared to M3. Thus, *La*GH13_20 will be more efficient in converting M4 to M2, whereas *La*GH13_31B most likely disproportionates M3 to M2 and to M4. The concerted action of both enzymes will mainly accumulate M2 from odd-numbered maltodextrins. The M2 product of these enzymes is phosphorolyzed by *La*GH65 to produce glucose (Glc) and Glc-1P, which are further catabolized in glycolysis (Fig. 6). Clearly, *La*GH13_31B contributes to the efficient catabolism of odd-numbered malto-

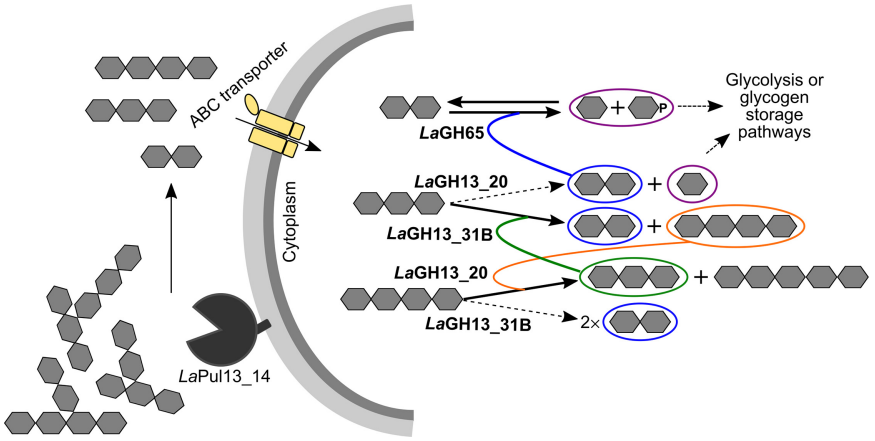

FIG 6 Schematic model of MOS catabolism in *L. acidophilus* NCFM. MOS produced from starch and glycogen degradation by human digestive enzymes, other bacteria, or by the extracellular pullulanase (*La*Pul13_14 [19]) are internalized by specific transporters. An ATP-binding cassette transporter is conserved in the locus in *Lactobacillus* but likely is defective in *L. acidophilus* NCFM due to a transposase (19). Odd-numbered MOS are degraded into M3, whereas even-numbered MOS are degraded to M2 by *La*GH13_20. While M3 is a poor substrate for *La*GH13_20, it is preferred by *La*GH13_31B. The action of *La*GH13_31B converts M3 into M2 and M4, which are the preferred substrates for *La*GH65 and *La*GH13_20, respectively. Products are either catabolized via glycolysis (20) or stored as glycogen (32).

dextrins through their disproportionation, resulting in larger, better substrates for *La*GH13_20 and M2, the preferred substrate for *La*GH65. This mode of catabolism of maltodextrins seems to be widely employed in *Firmicutes* but also in other bacteria, e.g., *Bifidobacterium*, where a different type of α-glucanotransferase is upregulated during growth on MOS (31). The advantages of having an extra extension step in the breakdown of maltodextrins combined with GH65 are not obvious compared to using α-glucosidases or phosphorylases, which directly break down maltodextrins. One possibility is that the extension of maltodextrins, especially during saturation with Glc and a lowered rate of *La*GH65 activity due to reverse phosphorolysis (20), serves as a transient energy reserve that is more rapidly mobilized than glycogen produced by this organism (32). The accumulation of M2 may also inhibit the activity of the maltogenic α-amylase. Further work is needed to verify this role.

Conclusions. This study provides biochemical data on a previously unknown subfamily of disproportionating enzymes conserved within the maltodextrin metabolism pathway in *Lactobacillus*. Kinetic analysis of the three 1,4-α-active enzymes involved in MOS utilization in *L. acidophilus* revealed that *La*GH13_31B acts as a pivot that may contribute to regulating MOS catabolism by allowing transient storage as longer MOS. We identified a unique signature of this subfamily comprising an insertion in a loop positioned in close proximity to the active-site cleft. This loop may act as a clamp that recognizes substrates, likely via aromatic stacking at a conserved aromatic side chain.

MATERIALS AND METHODS

Chemicals and carbohydrate substrates. High-purity (>95%) chemicals and commercial enzymes were from Sigma-Aldrich (MO, USA) unless otherwise stated. Glucose was purchased from VWR (PA, USA), and amylose (DP17) was purchased from Hayashibara Co. (Okayama, Japan).

Cloning, production, and purification of enzymes encoded by the MOS utilization gene cluster in *Lactobacillus acidophilus* NCFM. *L. acidophilus* NCFM genomic DNA, prepared as previously described (20), was used to clone the LBA1871 and LBA1872 genes (GenBank accession no. AAV43671.1 and AAV43672.1, respectively) in the pET-21a(+) and pET-28a(+) vectors (Novagen, Darmstadt, Germany), respectively, using primers listed in Table 2 and standard molecular biology protocols. The sequence-verified recombinant vectors, designated pET-21a(+)*La*GH13_20 and pET-28a(+)*La*GH13_31B for LBA1871 and LBA1872, respectively, were transformed into *Escherichia coli* production strain Rosetta (DE3) cells (Invitrogen). The production of the maltogenic α-amylase *La*GH13_20 and the oligosaccharide 1,4-α-glucosyltransferase *La*GH13_31B was carried out using a 5-liter bioreactor (Biostat B; B. Braun Biotech International, Melsungen, Germany) as previously described (33), with the exception of the induction conditions (optical density at 600 nm [OD_{600}] of 8, 18°C) and feed (linear gradient of

TABLE 2 Primers used for cloning and site-directed mutagenesis of enzymes

Target gene product	Primer sequence[a] (5′→3′)
*La*GH13_20	(+) CTA**GCTAGC**ATGCAATTAGCCGCTTTAAGACAC
	(−) CCG**CTCGAG**ATCAACCATGATTACAAAGCC
*La*GH13_31B	(+) GGAATTC**CATATG**TCACATTGGTACGATCATGC
	(−) CCG**CTCGAG**TTAATTCTCCTTTTTCAAAACAACACCCGCG
*La*GH13_31B Y295A	(+) AGAAGATGATTCCAAAATCGATAAGAGT*GCT*TCCGCACAATATCAGCCTA
	(−) TAGGCTGATATTGTGCGGA*AGC*ACTCTTATCGATTTTGGAATCATCTTCT

[a]Boldface indicates mutated bases, underlining indicates the changed codon, and italics indicate the changed base. (+), sense; (−), antisense.

8.4 to 15 ml h^{-1} in 5 h, and then 15 ml h^{-1} was maintained until harvest). The fermentation was harvested after 48 h of induction (OD_{600} of 50) by centrifugation (15,000 × *g* for 20 min at 4°C). Portions of 10-g cell pellets were resuspended in 50 ml BugBuster (BugBuster protein extraction reagent; Merck Millipore) supplemented with 5 μl Benzonase nuclease (Novagen) and incubated for 20 min at room temperature. Subsequently, the suspension was centrifuged (20,000 × *g* for 20 min), and the clarified supernatant was sterile filtered (0.45 μm) and used for purification. Both the *La*GH13_20 and *La*GH13_31B enzymes were purified by immobilized metal ion affinity chromatography on 5-ml HisTrap HP columns (GE Healthcare, Uppsala, Sweden) equilibrated with binding buffer (20 mM HEPES, 500 mM NaCl, 10 mM imidazole, 1 M $CaCl_2$, 10% glycerol, pH 7.5) and eluted with a linear gradient of imidazole from 10 mM to 300 mM over 35 CV at a flow rate of 1 ml min^{-1}. Fractions enriched with the enzymes were pooled, concentrated (30-kDa Amicon filter; Millipore), and applied to a HiLoad 26/60 Superdex 200 size exclusion column (GE Healthcare) at a flow rate of 0.5 ml min^{-1}. The purifications were performed on an ÄKTA Avant chromatograph (GE Healthcare), and pure enzyme fractions, analyzed by SDS-PAGE, were pooled, concentrated, and supplemented with 0.005% (wt/vol) NaN_3 after the determination of protein concentrations using UV absorbance (A_{280}; molar extinction coefficient [ε_{280}] of 113,220 M^{-1} cm^{-1}, predicted using the ExPASy server [34]). *La*GH65 was produced and purified as previously described (20) and further purified using size exclusion chromatography on a HiLoad 26/60 Superdex 75 column (GE Healthcare). The *La*GH13_31B Y295A variant was generated using primers listed in Table 2 and the QuikChange II site-directed mutagenesis kit (Agilent) with pET-28a(+)-*La*GH13_31B as the template. The mutant was produced at 0.5-liter scale using a 2-liter baffled shake flask and purified as described above.

DSC stability analysis. The differential scanning calorimetry (DSC) analysis was performed at protein concentrations of 1 mg ml^{-1} in 10 mM sodium phosphate buffer, 150 mM NaCl, pH 6.8, using a Nano DSC (TA instruments). Thermograms were recorded from 20 to 60°C at a scan speed of 1.5°C min^{-1} using buffer as a reference. The analysis was done in duplicates. Baseline-corrected data were analyzed using the NanoAnalyze software (TA instruments).

TLC of enzyme product profiles. Disproportionating abilities of *La*GH13_31B (0.5 μM) and *La*GH13_31B Y295A (0.5 μM) on M3 (10 mM) were visualized by thin-layer chromatography (TLC). Reactions mixtures (100 μl) were incubated in standard assay buffer at 37°C, and 2-μl aliquots were removed at appropriate time points and spotted on a silica gel 60 F454 plate (Merck). The separation was carried out in butanol-ethanol-MilliQ water (5:3:2) (vol/vol) as the mobile phase, and sugars were visualized with 5-methylresorcinol–ethanol-sulfuric acid (2:80:10) (vol/vol) and heat treatment.

Enzyme activity. Oligo-1,6-α-glucosidase activity by *La*GH13_31B (50 nM) was analyzed at pH 6.8 and 37°C for 12 min in 300-μl reaction mixtures containing isomaltose or panose (5 mM) in the assay buffer (10 mM morpholineethanesulfonic acid [MES], 150 mM NaCl, 0.005% Tween 20, pH 6.8). The liberated Glc was quantified using a modified glucose oxidase/peroxidase assay (GOPOD; Megazyme, Wicklow, Ireland) (21). Similarly, maltose phosphorolysis kinetics by *La*GH65 was analyzed with reaction mixtures containing M2 (0.63 to 20 mM) and *La*GH65 (23 nM) and the assay buffer (100 mM phosphate-citrate, 0.005% Tween 20). Aliquots (50 μl) were removed at five time points (3, 6, 9, 12, and 15 min) and added to 100 μl 2 M Tris-HCl, pH 7, to stop the reaction, and Glc was quantified as described above. The same assay was used to measure the hydrolysis kinetics of *La*GH13_20 on M3 (0.63 to 20 mM) and the disproportionation activity of *La*GH13_31B on M2 (1.6 to 300 mM), with the only exception being that *La*GH13_20 (70 nM) and *La*GH13_31B (6 μM) were incubated in the assay buffer (10 mM MES, 150 mM NaCl, 0.005% Tween 20, pH 6.8). The hydrolysis kinetics of *La*GH13_20 (7 nM) toward M4 (0.63 to 20 mM) and disproportionation kinetics of *La*GH13_31B (3.8 nM) on M3 (0.63 to 30 mM) were determined using a coupled assay, where 0.2 μM *La*GH65 and 20 mM phosphate were included in the assay buffer.

A similar assay was also applied to measure the disproportionation kinetics of M3 (0.63 to 40 mM) and M4 (1.3 to 40 mM) with 1.9 and 3.8 nM *La*GH13_31B, respectively, using HPAEC-PAD as described below. Appropriate amounts of reaction mixtures were diluted into 0.1 M NaOH before injection, and the separated saccharides were quantified based on peak areas. Glc, M2, and MOS (0.015 to 1 mM) were used as standards. The Michaelis-Menten model was fit to the initial rate data to derive kinetic parameters using OriginPro 2015 software (OriginLab, Northampton, MA). The utilization of MOS by *La*GH13_31B (3.8 nM) alone or by a mixture of *La*GH65 (3.8 nM), *La*GH13_20 (3.8 nM), and *La*GH13_31B (3.8 nM) toward 5 mM M3, M4, or M5 was also analyzed by HPAEC-PAD. Assay conditions similar to those described above

were applied, with the only exception being that samples were incubated for 24 h in the buffer of the coupled assay.

Relative disproportionation activities of *La*GH13_31 (60 μM) and *La*GH13_31 Y295A (114 μM) on M2 (100 mM) were analyzed as described above, using standard assay buffer (10 mM MES, 150 mM NaCl, 0.005% Tween 20, pH 6.8) and an incubation time of 10 min at 37°C. The liberated Glc was quantified using the coupled enzyme assay described above. The analysis was performed in technical triplicates. Relative activities of *La*GH13_31 (5 nM) and *La*GH13_31 Y295A (0.5 μM) toward M3 (5 mM) were assayed under similar reaction conditions. For determining initial rates, reactions (150 μl) were incubated for 8 min at 37°C, and aliquots of 15 μl were removed every minute and quenched in 135 μl 0.1 M NaOH. Reaction products were quantified using HPAEC-PAD as described in detail below. A similar assay was used to measure the disproportionation kinetics of *La*GH13_31 Y295A on M3 (1 to 60 mM), with the only exception being that a single aliquot was removed after 5 min of incubation before quenching in 0.1 M NaOH. The HPAEC-PAD analysis was performed in technical triplicates.

HPAEC-PAD. 1,6-α-Glucosidase activity and enzyme kinetics were analyzed using HPAEC-PAD analysis. Samples (10 μl) were injected into a Carbopac PA200 analytical column coupled with a guard column (Thermo Fisher Scientific, Sunnyvale, CA, USA) installed on an ICS-3000 chromatograph (Thermo Fisher Scientific) and analyzed at a flow rate of 0.35 ml min^{-1}. The elution was carried out using a constant concentration of 100 mM NaOH and, in addition, from 0 to 10 min a gradient of 40 to 150 mM sodium acetate (NaOAc); 10 to 11 min, 150 to 400 mM NaOAc; 11 to 15 min, 400 mM NaOAc; and 15 to 20 min, a linear gradient from 400 mM to initial conditions of 40 mM NaOAc. The system was interfaced using Chromeleon, version 6.7, which was also used to evaluate the chromatograms.

Sequence alignment and phylogenetic analysis. All lactobacillus protein sequences classified into GH13_31 in the CAZy database (12), together with the sequences of the GH13_31 members classified as characterized, were retrieved from the CAZy database. Redundancy of the protein sequences was reduced using the Decrease redundancy server (web.expasy.org/decrease_redundancy/) with 99% maximum identity as a rule to reduce redundancy. A structure-guided multiple-sequence alignment then was made using the PROMALS3D web server (35), including available structures of GH13_31 enzymes using default settings. Based on the structure-based multiple-sequence alignment, a phylogenetic tree was constructed using maximum likelihood based on conserved sites using the Jones, Taylor, and Thorton (JTT) model and with 500 bootstrap replications. Tree construction was done using MEGA X (36) and visualized using Dendroscope, version 3.6.3 (37). The multiple-sequence alignment was visualized using ESPript 3.0 (38).

The organization of the MOS gene cluster of different *Lactobacillus* strains was analyzed using the genome database provided by the National Center for Biotechnology Information (NCBI), MGcV (the microbial genomic context viewer for comparative genome analysis) (39), KEGG (Kyoto Encyclopedia of Genes and Genomes) (40), and previous studies (20, 41).

Crystallization, data collection, and structure determination. Screening for crystallization conditions was performed using 3.6 mg ml^{-1} *La*GH13_31B in 10 mM MES, pH 6.5, 10 mM NaCl, and 0.5 mM $CaCl_2$ by the sitting-drop vapor-diffusion method using the JCSG+ (Qiagen, Hilden, Germany), Index (Hampton Research, Aliso Viejo, CA, USA), and Morpheus MD1–46 (Molecular Dimensions, Newmarket, UK) screens. An Oryx8 liquid-handling robot (Douglas Instruments, Hungerford, UK) was used to set up the screens in MRC 2-drop plates (Douglas Instruments, Hungerford, UK) with a total drop volume of 0.3 μl and 3:1 and 1:1 ratios of protein solution and reservoir solution at room temperature. Small, thin-needle crystals appeared within 2 weeks at room temperature with a reservoir containing an equimolar mixture (0.02 M [each] sodium L-glutamate, DL-alanine, glycine, DL-lysine HCl, and DL-serine), buffer system 3, pH 8.5 (0.1 M bicine and 0.1 M Trizma base), 20% (vol/vol) polyethylene glycol 500 (PEG 500) methyl ether, and 10% (wt/vol) PEG 20000, pH 8.5 (Morpheus), in a protein-reservoir (1:1) droplet. Microseed matrix screening using the above-described needles (42) was performed in several of the above-described screens, but suitable crystals only appeared under the same conditions for several of those screens. No extra cryoprotection was used before the crystals were mounted and flash-frozen in liquid nitrogen. Diffraction data were collected at the ESRF beamline ID23-1 and processed with the XDS package (43) in space group $P2_1$ to 2.8 Å, with cell and processing statistics reported in Table 3. Molecular replacement was carried out in Molrep (44) with the structure of a GH13_31 oligo-1,6-α-glucosidase (PDB entry 1UOK) as the model, and 2 molecules/asymmetric unit were identified, as suggested by Matthew's number. The electron density generated from the solution showed a Ca^{2+} binding site, absent from the search model but present in several homologues. Several areas, especially in loop regions, initially had extremely poor density. The structure was refined using both Phenix (45) and REFMAC 5.0 (46) and with the aid of average maps from COOT (47), especially at the initial stages of model building and refinement, whereas several autobuild strategies in phenix, jelly-body, and ProSmart restrained refinement (using GH13_31 structures with PDB entries 4AIE and 4MB1) in REFMAC 5.0 were applied for the last stages. Noncrystallographic symmetry (NCS) restraints were used for most of the structure. The loop region 286 to 295 (comprising part of the unique loop containing Y295) could not be modeled confidently, although some residual density is clearly seen in this region (Fig. 2B). No density was visible for loop 519 to 522. Other regions have poor density in one of the two copies in the asymmetric unit, and here the area has been modeled similarly to the corresponding regions in the other chain, in which the density is considerably better. Structures were visualized with PyMOL, version 2.1.1 (Schrödinger, LLC).

Data availability. The plasmids used for the expression of the three enzymes characterized in the present study are in the collection of the authors and will be made available upon request. The structural

TABLE 3 Crystallographic data collection and refinement statistics

Parameter	Value
PDB no.	6Y9T
Wavelength (Å)	0.999870
Space group	$P2_1$
Unit cell parameter (Å)	
a	73.21
b	105.30
c	92.23
β (°)	96.95
No. of unique reflections	34,239
Resolution (Å)	50.00–2.78 (2.95–2.78)
Completeness (%)	97.3 (84.3)
Redundancy	5.1
Mean $I/\sigma(I)$	8.01 (0.83)
R_{meas} (%)	19.7 (198.9)
$CC_{1/2}$ (%)	99.4 (59.8)
R (%)	25.8
R_{free} (%)	33.6
RMSD[a] bonds (Å)	0.012
RMSD angles (°)	1.561
Molprobity combined score (90th percentile)	2.53
Molprobity Ramachandran (%)	
Favored	91.78
Outliers	0.94
Avg B-factors (Å^2)	86.2

[a]RMSD, root mean square deviation.

model coordinates for *La*GH13_31B and processed diffraction data have been deposited in the Protein Data Bank under accession number 6Y9T.

SUPPLEMENTAL MATERIAL

Supplemental material is available online only.

SUPPLEMENTAL FILE 1, PDF file, 4.4 MB.

ACKNOWLEDGMENTS

Mette Pries (Technical University of Denmark) and Dorte Boelskifte (University of Copenhagen) are thanked for technical assistance.

This work was supported by a Ph.D. scholarship from the Technical University of Denmark to S.A. and a FøSu grant from the Danish Strategic Research Council to the project "Gene discovery and molecular interactions in prebiotics/probiotics systems. Focus on carbohydrate prebiotics." The Carlsberg Foundation is acknowledged for an instrument grant that funded the DSC equipment. The Danish Ministry of Higher Education and Science, through the Instrument Center DANSCATT, funded travel to synchrotrons.

The crystallographic experiments were performed on beamline ID23-1 at the European Synchrotron Radiation Facility (ESRF), Grenoble, France. We are grateful to the ESRF staff for assistance.

REFERENCES

1. Muegge BD, Kuczynski J, Knights D, Clemente JC, Gonzalez A, Fontana L, Henrissat B, Knight R, Gordon JI. 2011. Diet drives convergence in gut microbiome functions across mammalian phylogeny and within humans. Science 332:970–974. https://doi.org/10.1126/science.1198719.
2. Thaiss CA, Zmora N, Levy M, Elinav E. 2016. The microbiome and innate immunity. Nature 535:65–74. https://doi.org/10.1038/nature18847.
3. Spanogiannopoulos P, Bess EN, Carmody RN, Turnbaugh PJ. 2016. The microbial pharmacists within us: a metagenomic view of xenobiotic metabolism. Nat Rev Microbiol 14:273–287. https://doi.org/10.1038/nrmicro.2016.17.
4. Flint HJ, Bayer EA, Rincon MT, Lamed R, White BA. 2008. Polysaccharide utilization by gut bacteria: potential for new insights from genomic analysis. Nat Rev Microbiol 6:121–131. https://doi.org/10.1038/nrmicro1817.
5. David LA, Maurice CF, Carmody RN, Gootenberg DB, Button JE, Wolfe BE, Ling AV, Devlin AS, Varma Y, Fischbach MA, Biddinger SB, Dutton RJ, Turnbaugh PJ. 2014. Diet rapidly and reproducibly alters the human gut microbiome. Nature 505:559–563. https://doi.org/10.1038/nature12820.
6. Donaldson GP, Lee SM, Mazmanian SK. 2016. Gut biogeography of the bacterial microbiota. Nat Rev Microbiol 14:20–32. https://doi.org/10.1038/nrmicro3552.

7. Sanders ME, Klaenhammer TR. 2001. Invited review: the scientific basis of *Lactobacillus acidophilus* NCFM functionality as a probiotic. J Dairy Sci 84:319–331. https://doi.org/10.3168/jds.S0022-0302(01)74481-5.
8. Lyra A, Hillilä M, Huttunen T, Männikkö S, Taalikka M, Tennilä J, Tarpila A, Lahtinen S, Ouwehand AC, Veijola L. 2016. Irritable bowel syndrome symptom severity improves equally with probiotic and placebo. World J Gastroenterol 22:10631–10642. https://doi.org/10.3748/wjg.v22.i48.10631.
9. Altermann E, Russell WM, Azcarate-Peril MA, Barrangou R, Buck BL, McAuliffe O, Souther N, Dobson A, Duong T, Callanan M, Lick S, Hamrick A, Cano R, Klaenhammer TR. 2005. Complete genome sequence of the probiotic lactic acid bacterium *Lactobacillus acidophilus* NCFM. Proc Natl Acad Sci U S A 102:3906–3912. https://doi.org/10.1073/pnas.0409188102.
10. Ouwehand AC, Tiihonen K, Saarinen M, Putaala H, Rautonen N. 2009. Influence of a combination of *Lactobacillus acidophilus* NCFM and lactitol on healthy elderly: intestinal and immune parameters. Br J Nutr 101:367–375. https://doi.org/10.1017/S0007114508003097.
11. Magro DO, De Oliveira LMR, Bernasconi I, Ruela MDS, Credidio L, Barcelos IK, Leal RF, Ayrizono M, Fagundes JJ, Teixeira LDB, Ouwehand AC, Coy C. 2014. Effect of yogurt containing polydextrose, *Lactobacillus acidophilus* NCFM and *Bifidobacterium lactis* HN019: a randomized, double-blind, controlled study in chronic constipation. Nutr J 13:75. https://doi.org/10.1186/1475-2891-13-75.
12. Lombard V, Ramulu HG, Drula E, Coutinho PM, Henrissat B. 2014. The carbohydrate-active enzymes database (CAZy) in 2013. Nucleic Acids Res 42:490–495. https://doi.org/10.1093/nar/gkt1178.
13. Andersen JM, Barrangou R, Abou Hachem M, Lahtinen S, Goh YJ, Svensson B, Klaenhammer TR. 2011. Transcriptional and functional analysis of galactooligosaccharide uptake by *lacS* in *Lactobacillus acidophilus*. Proc Natl Acad Sci U S A 108:17785–17790. https://doi.org/10.1073/pnas.1114152108.
14. Andersen JM, Barrangou R, Abou Hachem M, Lahtinen SJ, Goh Y-J, Svensson B, Klaenhammer TR. 2012. Transcriptional analysis of prebiotic uptake and catabolism by *Lactobacillus acidophilus* NCFM. PLoS One 7:e44409. https://doi.org/10.1371/journal.pone.0044409.
15. Theilmann MC, Goh YJ, Nielsen KF, Klaenhammer TR, Barrangou R, Abou Hachem M. 2017. *Lactobacillus acidophilus* metabolizes dietary plant glucosides and externalizes their bioactive phytochemicals. mBio 8:e01421-17. https://doi.org/10.1128/mBio.01421-17.
16. Bertoft E. 2017. Understanding starch structure: recent progress. Agronomy 7:56. https://doi.org/10.3390/agronomy7030056.
17. Ze X, Duncan SH, Louis P, Flint HJ. 2012. *Ruminococcus bromii* is a keystone species for the degradation of resistant starch in the human colon. ISME J 6:1535–1543. https://doi.org/10.1038/ismej.2012.4.
18. Cockburn DW, Orlovsky NI, Foley MH, Kwiatkowski KJ, Bahr CM, Maynard M, Demeler B, Koropatkin NM. 2015. Molecular details of a starch utilization pathway in the human gut symbiont *Eubacterium rectale*. Mol Microbiol 95:209–230. https://doi.org/10.1111/mmi.12859.
19. Møller MS, Goh YJ, Rasmussen KB, Cypryk W, Celebioglu HU, Klaenhammer TR, Svensson B, Abou Hachem M. 2017. An extracellular cell-attached pullulanase confers branched α-glucan utilization in human gut *Lactobacillus acidophilus*. Appl Environ Microbiol 83:e00402-17. https://doi.org/10.1128/AEM.00402-17.
20. Nakai H, Baumann MJ, Petersen BO, Westphal Y, Schols H, Dilokpimol A, Hachem MA, Lahtinen SJ, Duus JØ, Svensson B. 2009. The maltodextrin transport system and metabolism in *Lactobacillus acidophilus* NCFM and production of novel α-glucosides through reverse phosphorolysis by maltose phosphorylase. FEBS J 276:7353–7365. https://doi.org/10.1111/j.1742-4658.2009.07445.x.
21. Møller MS, Fredslund F, Majumder A, Nakai H, Poulsen J-C, Lo Leggio L, Svensson B, Abou Hachem M. 2012. Enzymology and structure of the GH13_31 glucan 1,6-α-glucosidase that confers isomaltooligosaccharide utilization in the probiotic *Lactobacillus acidophilus* NCFM. J Bacteriol 194:4249–4259. https://doi.org/10.1128/JB.00622-12.
22. Auiewiriyanukul W, Saburi W, Kato K, Yao M, Mori H. 2018. Function and structure of GH13_31 α-glucosidase with high α-(1$\rightarrow$4)-glucosidic linkage specificity and transglucosylation activity. FEBS Lett 592:2268–2281. https://doi.org/10.1002/1873-3468.13126.
23. Shirai T, Hung VS, Morinaka K, Kobayashi T, Ito S. 2008. Crystal structure of GH13 α-glucosidase GSJ from one of the deepest sea bacteria. Proteins 73:126–133. https://doi.org/10.1002/prot.22044.
24. Oslancová A, Janecek S. 2002. Oligo-1,6-glucosidase and neopullulanase enzyme subfamilies from the α-amylase family defined by the fifth conserved sequence region. Cell Mol Life Sci 59:1945–1959. https://doi.org/10.1007/pl00012517.
25. Joyet P, Mokhtari A, Riboulet-Bisson E, Blancato VS, Espariz M, Magni C, Hartke A, Deutscher J, Sauvageot N. 2017. Enzymes required for maltodextrin catabolism in *Enterococcus faecalis* exhibit novel activities. Appl Environ Microbiol 83:e00038-17. https://doi.org/10.1128/AEM.00038-17.
26. Janeček Š. 2002. How many conserved sequence regions are there in the α-amylase family? Biologia 57:29–41.
27. Roujeinikova A, Raasch C, Sedelnikova S, Liebl W, Rice DW. 2002. Crystal structure of *Thermotoga maritima* 4-α-glucanotransferase and its acarbose complex: implications for substrate specificity and catalysis. J Mol Biol 321:149–162. https://doi.org/10.1016/s0022-2836(02)00570-3.
28. Jung J-H, Jung T-Y, Seo D-H, Yoon S-M, Choi H-C, Park BC, Park C-S, Woo E-J. 2011. Structural and functional analysis of substrate recognition by the 250s loop in amylomaltase from *Thermus brockianus*. Proteins 79:633–644. https://doi.org/10.1002/prot.22911.
29. Weiss SC, Skerra A, Schiefner A. 2015. Structural basis for the interconversion of maltodextrins by MalQ, the amylomaltase of *Escherichia coli*. J Biol Chem 290:21352–21364. https://doi.org/10.1074/jbc.M115.667337.
30. O'Neill EC, Stevenson CEM, Tantanarat K, Latousakis D, Donaldson MI, Rejzek M, Nepogodiev SA, Limpaseni T, Field RA, Lawson DM. 2015. Structural dissection of the maltodextrin disproportionation cycle of the *Arabidopsis* plastidial enzyme DPE1. J Biol Chem 290:29834–29853. https://doi.org/10.1074/jbc.M115.682245.
31. Andersen JM, Barrangou R, Abou Hachem M, Lahtinen SJ, Goh YJ, Svensson B, Klaenhammer TR. 2013. Transcriptional analysis of oligosaccharide utilization by *Bifidobacterium lactis* Bl-04. BMC Genomics 14:312. https://doi.org/10.1186/1471-2164-14-312.
32. Goh YJ, Klaenhammer TR. 2014. Insights into glycogen metabolism in *Lactobacillus acidophilus*: impact on carbohydrate metabolism, stress tolerance and gut retention. Microb Cell Fact 13:94. https://doi.org/10.1186/s12934-014-0094-3.
33. Fredslund F, Abou Hachem M, Jonsgaard Larsen R, Gerd Sørensen P, Coutinho PM, Lo Leggio L, Svensson B. 2011. Crystal structure of α-galactosidase from *Lactobacillus acidophilus* NCFM: insight into tetramer formation and substrate binding. J Mol Biol 412:466–480. https://doi.org/10.1016/j.jmb.2011.07.057.
34. Gasteiger E, Gattiker A, Hoogland C, Ivanyi I, Appel RD, Bairoch A. 2003. ExPASy: the proteomics server for in-depth protein knowledge and analysis. Nucleic Acids Res 31:3784–3788. https://doi.org/10.1093/nar/gkg563.
35. Pei J, Kim B-H, Grishin NV. 2008. PROMALS3D: a tool for multiple protein sequence and structure alignments. Nucleic Acids Res 36:2295–2300. https://doi.org/10.1093/nar/gkn072.
36. Kumar S, Stecher G, Li M, Knyaz C, Tamura K. 2018. MEGA X: molecular evolutionary genetics analysis across computing platforms. Mol Biol Evol 35:1547–1549. https://doi.org/10.1093/molbev/msy096.
37. Huson DH, Scornavacca C. 2012. Dendroscope 3: an interactive tool for rooted phylogenetic trees and networks. Syst Biol 61:1061–1067. https://doi.org/10.1093/sysbio/sys062.
38. Robert X, Gouet P. 2014. Deciphering key features in protein structures with the new ENDscript server. Nucleic Acids Res 42:W320–W324. https://doi.org/10.1093/nar/gku316.
39. Overmars L, Kerkhoven R, Siezen RJ, Francke C. 2013. MGcV: the microbial genomic context viewer for comparative genome analysis. BMC Genomics 14:209. https://doi.org/10.1186/1471-2164-14-209.
40. Kanehisa M, Goto S, Hattori M, Aoki-Kinoshita KF, Itoh M, Kawashima S, Katayama T, Araki M, Hirakawa M. 2006. From genomics to chemical genomics: new developments in KEGG. Nucleic Acids Res 34:D354–D357. https://doi.org/10.1093/nar/gkj102.
41. Monedero V, Yebra MJ, Poncet S, Deutscher J. 2008. Maltose transport in *Lactobacillus casei* and its regulation by inducer exclusion. Res Microbiol 159:94–102. https://doi.org/10.1016/j.resmic.2007.10.002.
42. D'Arcy A, Bergfors T, Cowan-Jacob SW, Marsh M. 2014. Microseed matrix screening for optimization in protein crystallization: what have we learned? Acta Crystallogr F Struct Biol Commun 70:1117–1126. https://doi.org/10.1107/S2053230X14015507.
43. Kabsch W. 2010. XDS. Acta Crystallogr D Biol Crystallogr 66:125–132. https://doi.org/10.1107/S0907444909047337.
44. Vagin A, Teplyakov A. 2010. Molecular replacement with MOLREP. Acta Crystallogr D Biol Crystallogr 66:22–25. https://doi.org/10.1107/S0907444909042589.
45. Adams PD, Afonine PV, Bunkóczi G, Chen VB, Davis IW, Echols N, Headd JJ, Hung L-W, Kapral GJ, Grosse-Kunstleve RW, McCoy AJ, Moriarty NW, Oeffner R, Read RJ, Richardson DC, Richardson JS, Terwilliger TC, Zwart

PH. 2010. PHENIX: a comprehensive Python-based system for macromolecular structure solution. Acta Crystallogr D Biol Crystallogr 66:213–221. https://doi.org/10.1107/S0907444909052925.
46. Nicholls RA, Long F, Murshudov GN. 2013. Recent advances in low resolution refinement tools in REFMAC5, p 231–258. *In* Read R, Urzhumtsev AG, Lunin VY (ed), Advancing methods for biomolecular crystallography. Springer, Dordrecht, Netherlands.
47. Emsley P, Lohkamp B, Scott WG, Cowtan K. 2010. Features and development of Coot. Acta Crystallogr D Biol Crystallogr 66:486–501. https://doi.org/10.1107/S0907444910007493.
48. MacGregor EA, Janecek S, Svensson B. 2001. Relationship of sequence and structure to specificity in the α-amylase family of enzymes. Biochim Biophys Acta 1546:1–20. https://doi.org/10.1016/S0167-4838(00)00302-2.